

# Magnetotelluric Investigations of Geothermal Systems Centred in Southern British Columbia (Parts of NTS 082, 083, 092, 093)

C. Hanneson<sup>1</sup>, Department of Physics, University of Alberta, Edmonton, Alberta, cedar@ualberta.ca

M.J. Unsworth, Department of Physics and Department of Earth and Atmospheric Sciences, University of Alberta, Edmonton, Alberta

Hanneson, C. and Unsworth, M.J. (2022): Magnetotelluric investigations of geothermal systems centred in southern British Columbia (parts of NTS 082, 083, 092, 093); in Geoscience BC Summary of Activities 2021: Energy and Water, Geoscience BC, Report 2022-02, p. 81–94.

## Introduction

British Columbia (BC) has a range of significant geothermal resources in settings that include volcanic systems, fault-hosted systems and hot dry rock. Volcanic systems are found in the Garibaldi volcanic belt (GVB), including at Mount Meager, and fault-hosted systems are found near the southern Rocky Mountain Trench (SRMT). Both fault-hosted geothermal systems and hot dry rock resources are found in the Columbia Mountains.

Geophysical exploration using electromagnetic (EM) methods—including magnetotelluric (MT) surveys—is widely used in geothermal studies. These methods have been used to investigate two areas in southern BC, at different spatial scales:

- 1) Southeastern BC: a regional study at a large spatial resolution with horizontal model discretization of 5 km. This study had the aim of correlating regional-scale crustal structures with small-scale geothermal systems.
- 2) Mount Meager: a study surrounding the Mount Meager massif at a smaller spatial resolution with horizontal model discretization of 250 m. This study had the aim of imaging deep hydrothermal systems and magma bodies associated with a Holocene volcanic centre.

The study of the Mount Meager volcanic system is part of a multidisciplinary research program (the Garibaldi volcanic belt geothermal energy project) that includes magnetotelluric, passive seismic and gravity surveys, bedrock mapping, fracture analysis, and thermal-spring geochemistry (Grasby et al., 2020).

## Tectonic and Geological Settings

The studied areas are located in the Canadian Cordillera and adjacent Western Canada Sedimentary Basin (WCSB);

Figure 1). The Cordillera is an orogenic belt that covers much of BC and Yukon, as well as the western edges of Alberta and the Northwest Territories, and it is commonly divided into five morphogeological belts based on bedrock type and geomorphology. From west to east, they are: 1) the Insular Belt, 2) the Coast Belt, 3) the Intermontane Belt, 4) the Omineca Belt, and 5) the Foreland Belt. The SRMT separates the Omineca and Foreland belts.

The Juan de Fuca Plate, situated offshore southwestern BC and northwestern Washington, subducts beneath the North American Plate at the Cascadia subduction zone (Figure 1). The tectonic convergence rate between these two plates is ~40 mm/year (Kreemer et al., 2014). Dehydration of the subducting slab releases volatiles into the overlying mantle of the North American Plate, lowering its melting point and creating a region of partial melt, which leads to volcanism at the surface (Stern, 2002). The chain of volcanoes resulting from this subduction is called the Cascade volcanic arc.

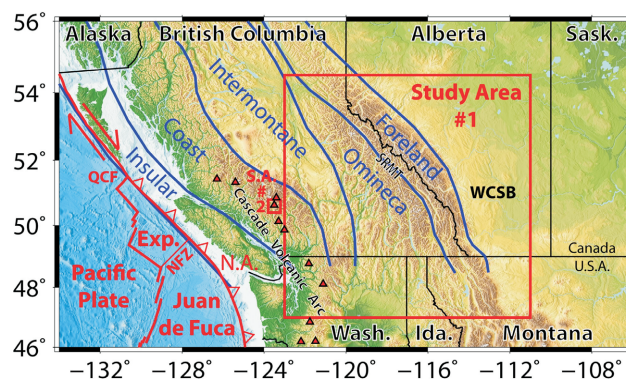


**Figure 1.** Southwestern Canada and northwestern United States showing the two study areas (red boxes). Study area 1 is centred on southeastern British Columbia but extends east into the province of Alberta and south into the states of Washington, Idaho and Montana. Study area 2 is centred on Mount Meager in the Cascade volcanic arc. Provincial, state and federal boundaries (black lines), morphogeological boundaries (blue lines), plate boundaries (red lines) and major volcanic centres (red triangles) are also shown. Abbreviations: Exp., Explorer Plate; Ida., Idaho; N.A., North American Plate; NFZ, Nootka fault zone; QCF, Queen Charlotte fault; S.A., study area; Sask., Saskatchewan; SRMT, southern Rocky Mountain Trench; Wash., Washington; WCSB, Western Canada Sedimentary Basin.

<sup>1</sup>The lead author is a 2021 Geoscience BC Scholarship recipient.

This publication is also available, free of charge, as colour digital files in Adobe Acrobat® PDF format from the Geoscience BC website: <http://geosciencebc.com/updates/summary-of-activities/>.

The northernmost segment of the Cascade volcanic arc (north of latitude 48°N) trends roughly northwest, whereas the rest of the arc trends generally north. The former, extending from Glacier Peak to Silverthorne Caldera, is the GVB (Figure 2); the latter (south of the area shown in Figure 2), from Mount Rainier in central Washington to Mount Lassen in northern California, is called the High Cascades (Mullen et al., 2017). North of the Nootka fault zone (Figure 1), the plate boundary transitions from convergent to transform, with strike-slip motion occurring north of the Queen Charlotte fault, and the Cascade volcanic arc dies out. In contrast to the Juan de Fuca Plate, the Explorer Plate is subducting at a rate of only 5–20 mm/year (Hutchinson et al., 2020).

### Magnetotelluric Theory

The MT method uses natural EM signals to image the electrical resistivity of the subsurface and is widely used in geothermal exploration (Muñoz, 2014). The low-frequency radio wave sources are generated by global lightning activity and interactions between solar wind and the Earth’s ionosphere. This EM method measures time series of electric and magnetic fields at the surface of the Earth, then converts them into frequency-domain transfer functions that describe the impedance of the Earth. The impedance ( $Z$ ) as a function of angular frequency,  $\omega$ , is defined as a 2 by 2 tensor with  $Z_{ij}(\omega) = E_i(\omega)/H_j(\omega)$  for  $i, j = \{x, y\}$ , where  $E$  is the electric field strength and  $H$  is the magnetic field strength. The vertical magnetic transfer function, referred to as the tipper ( $T$ ), is defined as a vector with  $T_{zk}(\omega) = H_z(\omega)/H_k(\omega)$  for  $k = \{x, y\}$ . These transfer functions are used to calculate the electrical resistivity at depth. The theoretical foundations of the MT method were developed by Cagniard (1953) and a detailed description is given by Chave and Jones (2012).

The MT method has two main advantages that make it suitable for geothermal exploration:

- 1) It can effectively image aqueous and magmatic fluids, both of which are relevant to geothermal exploration. The electrical resistivity of the crust varies over several orders of magnitude: dry crystalline rock has a resistivity in excess of 1000  $\Omega \cdot m$ , whereas the presence of aqueous fluids or partial melt can lower this to values in the range 1–10  $\Omega \cdot m$ . Thus, MT data can help distinguish fluid-rich zones.
- 2) It can resolve crustal features over a broad range of depths, allowing for investigation of both fine-scale crustal structure and deeper resistivity anomalies.

lies. The frequency of the passive radio-wave source controls the depth of exploration according to the skin depth ( $\delta$ ), which is defined in metres as  $\delta \approx 500(\rho T)^{1/2}$ , where  $\rho$  is the bulk resistivity and  $T$  is the period of the signal. Therefore, longer periods give information about deeper structures and signals are more attenuated in lower resistivity materials. This broad depth range is a distinct advantage over other EM methods that are more limited in scale.

Resistivity models derived from MT data are an excellent way to detect fluids in bedrock during geothermal exploration; however, there are other causes of low resistivity in the near surface and all possible explanations must be considered in a program of geothermal exploration. These include presence of hydrothermal alteration minerals (Ussher et al., 2000; Hersir et al., 2015), graphite films (Frost et al., 1989) and sulphide minerals (Varentsov et al., 2013). Additional geophysical and geological data are helpful in distinguishing between different low-resistivity materials.

The techniques available for the analysis of MT data have drastically improved over the past decade due to increased computing power. In the past, one-dimensional and two-dimensional (1-D and 2-D) inversions were used to derive models of subsurface resistivity from MT data, but this greatly limited the application of the method in complex geological environments. Magnetotelluric data can now be inverted to produce three-dimensional (3-D) resistivity models using new inversion codes that are run on multiprocessor clusters (Kelbert et al., 2014; Lindsey and Newman, 2015). Topography can be modelled in 3-D and recent advances have allowed 3-D anisotropy to be modelled as well (Kong et al., 2021).

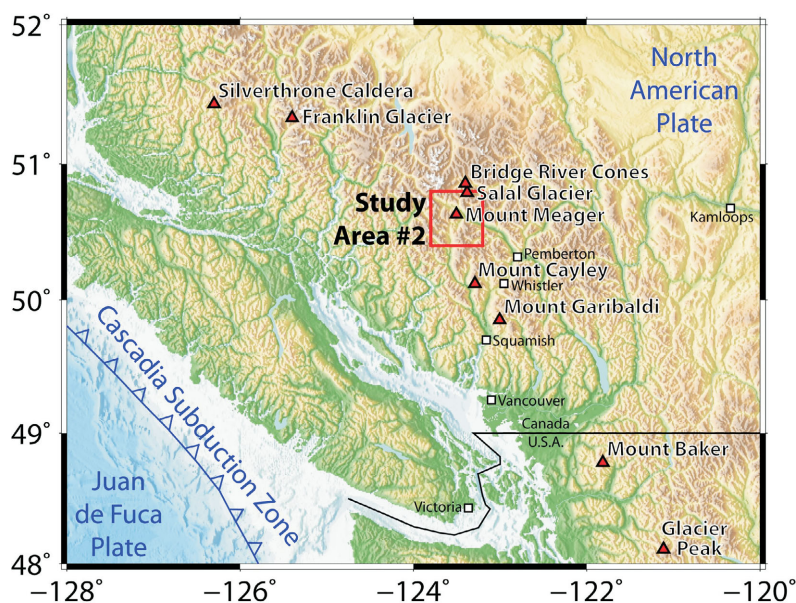


**Figure 2.** Southwestern British Columbia and northwestern Washington showing study area 2. Major volcanic centres of the Garibaldi volcanic belt are shown as red triangles, cities and towns are shown as squares.

## Study Area 1: Southeastern BC

### Geothermal Background

Study area 1 is centred on the SRMT, a major fault-controlled valley in southeastern BC. The region surrounding the SRMT is characterized by relatively high heat flow ( $\sim 75 \text{ mW/m}^2$ ), and surface geothermal features such as the Radium and Fairmont hot springs occur along the valley floor, making it a promising target for exploration for geothermal resources. Faults that occur within and adjacent to the SRMT include: the SRMT fault, Purcell thrust fault, Redwall fault and Lussier fault (Figure 3). The SRMT fault underlies the SRMT for much of its length, though there are limited outcrop exposures of the fault itself. The fault dips steeply west and estimates of normal dip-slip displacement range from 2 to 10 km (McDonough and Simony, 1988; Gal and Ghent, 1990; van der Velden and Cook, 1996). The across-fault continuity of several transverse features, both structural and stratigraphic, indicate that it does not exhibit significant strike-slip offset (McMechan and Thompson, 1989), though Finley (2020) suggested the possibility of post-Eocene dextral offset on the order of tens of kilometres. The Purcell thrust fault lies within the SRMT from latitude  $51.5^\circ\text{N}$  (north of Golden) to latitude  $50.5^\circ\text{N}$  (near Invermere). This fault is regarded as an out-of-sequence thrust fault that developed during the last stages of Mesozoic compression. Notably, no thermal springs occur along the SRMT where the Purcell thrust occurs, suggesting this structure may not be conducive to fluid circulation or that there is limited fluid supply at depth.

The Redwall and Lussier faults are parallel to and east of the SRMT, between the towns of Radium and Cranbrook. The nature of these faults is not well understood, and they have variably been interpreted as dextral, sinistral or thrust faults (North and Henderson, 1954; Charlesworth, 1959; Foo, 1979). Many thermal springs near the southern portion of the SRMT in fact coincide with these faults rather than the SRMT fault itself, hence their inclusion in this study.

Within study area 1, MT data collected at more than 300 locations during the current and previous studies cover mainly the Omineca, Foreland and Intermontane belts of the Canadian Cordillera (Figure 3). In this region, heat flow is anomalously high,  $70\text{--}120 \text{ mW/m}^2$ , compared with the national average of  $64 \pm 16 \text{ mW/m}^2$  (Majorowicz and Grasby, 2010). For comparison, an average of  $85\text{--}90 \text{ mW/m}^2$  is observed in the Basin and Range province to the south, which hosts many of the United States' high-temperature ( $>150^\circ\text{C}$ ) geothermal systems (Wisian and Blackwell, 2004). The presence of more than 40 thermal springs within study area 1 is suggestive of the region's geothermal potential.

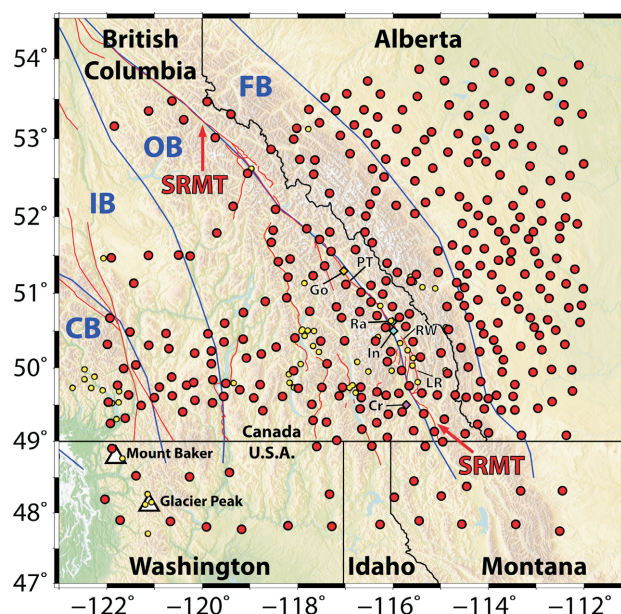


**Figure 3.** Magnetotelluric stations (red dots) used in the geophysical inversion to produce the electrical resistivity model shown in Figures 6 and 7. The approximate extent of the southern Rocky Mountain Trench is indicated by the red arrows. Provincial, state and federal boundaries (black lines), morphogeological boundaries (blue lines), major faults (red lines), Cascade arc volcanoes (white triangles), thermal springs (yellow dots) and population centres mentioned in the text (coloured diamonds) are also shown. Abbreviations: CB, Coast Belt; Cr, Cranbrook; FB, Foreland Belt; Go, Golden; IB, Intermontane Belt; In, Invermere; LR, Lussier River fault; OB, Omineca Belt; PT, Purcell thrust fault; Ra, Radium; RW, Redwall fault; SRMT, southern Rocky Mountain Trench.

It has previously been suggested that the locations of these thermal springs are controlled by faults (Grasby and Hutcheon, 2001) that allow deep circulation and consequent heating of meteoric water. Thermal springs in this study area include the Wolfenden, Radium, Fairmont, Red Rock, Lussier, Ram Creek and Wildhorse hot springs near the SRMT (Grasby and Hutcheon, 2001; Allen et al., 2006). Aqueous geothermometry has indicated that the spring water reaches temperatures of  $\sim 40\text{--}100^\circ\text{C}$ , implying circulation depths of  $\sim 2\text{--}5 \text{ km}$  (Grasby and Hutcheon, 2001). Although these temperatures are on the lower limit of what can be used to efficiently produce electricity, there is interest in using these systems for direct-use geothermal heating (Tuya Terra Geo Corp. and Geothermal Management Company, Inc., 2016). It is also important to note that convection and advection can have a cooling effect and may lower geothermal resource potential; therefore, thermal springs do not always indicate high geothermal potential (Grasby and Ferguson, 2010).

### Data and Methods

Study 1 used data from 336 MT sites in an area spanning from latitude  $47.7$  to  $54^\circ\text{N}$  and longitude  $112$  to  $122^\circ\text{W}$  (Figure 3). These data included 110 LITHOPROBE sites, 22 EarthScope USArray sites and 19 sites from other previ-

ous studies. The University of Alberta MT research group collected an additional 185 MT soundings between 2002 and 2018. The large extent of the grid (i.e., extending south into the United States and east almost to the Saskatchewan border) enhances the model precision in southeastern BC, our area of interest, by extending the data coverage beyond the southern Omineca Belt on all four sides. In previous decades, inversion of MT data was limited to 1-D and 2-D, producing resistivity models that were limited in their ability to adequately represent Earth structure. The development of new inversion algorithms that run on multiprocessor clusters has allowed 3-D inversion to become practical in recent years. The MT transfer functions (impedance and tipper) were jointly inverted using the ModEM algorithm (Kelbert et al., 2014). The inversion used data at 18 periods, logarithmically spaced between 1 and 18 000 s. Tipper data were omitted at the two longest periods; when they were included, they resulted in the highest misfit of any single-component single-period misfit. Furthermore, Meqbel et al. (2014) omitted tipper data at periods longer than 6500 s to avoid external source bias, which aligns with our methods.

The 336 sites were chosen from a total of more than 700 based on the high quality of their data and to ensure that station spacing was as uniform as possible. The median distance between a station and its nearest neighbour was 22 km. The data were measured in geomagnetic co-ordinates: magnetic north and east for  $x$  and  $y$ , respectively. For the inversion, the data were rotated to a geographic co-ordinate system: geographic north and east for  $x$  and  $y$ , respectively. The following error floors were applied to the impedance ( $\mathbf{Z}$ ) and tipper ( $\mathbf{T}$ ) data: 5% of  $(|Z_{xy}|/|Z_{yx}|)^{1/2}$  to  $Z_{xy}$  and  $Z_{yx}$ , 10% of  $(|Z_{xy}|/|Z_{yx}|)^{1/2}$  to  $Z_{xx}$  and  $Z_{yy}$ , and 0.03 to  $T_{zx}$  and  $T_{zy}$ , where  $\mathbf{Z}$  is a complex-valued 2 by 2 tensor and  $\mathbf{T}$  is a complex-valued 2 by 1 vector. These are the same error floors used by Wang (2019).

Study area 1 was approximately 700 km by 700 km; therefore, a relatively coarse mesh was used, as explained below. The model cells were 5 km by 5 km in the horizontal plane, with 12 padding cells increasing geometrically by a factor of 1.4 away from the central grid. Given the areal extent of the study area, this was the finest grid that could be modelled using a reasonable amount of memory on a parallel computing cluster; the inversion required roughly 500 GB of memory for nearly four weeks. During data selection, locations were chosen to ensure that a minimum of two vacant grid cells separated any two MT sites. The uppermost layer was 50 m thick, and the layer thickness increased geometrically by a factor of 1.15 downward. The total model volume was 2689 km from north to south, 2709 km from east to west, and 1105 km from surface to base, allowing for a significant buffer around the study area. At the longest period in our dataset, the skin depth in a 100  $\Omega\cdot\text{m}$  half-space is 679 km; therefore, the model extended approximately 1.5

skin depths in all directions. Due to the coarseness of the mesh and the computing resources needed, topography and bathymetry were not included in the model. The 3-D rectangular model mesh used for this study had 1.76 million cells: 172 in the north-south direction, 176 in the east-west direction, and 58 in the vertical direction.

Model covariance length scale,  $\gamma$ , is a measure of model smoothing applied across cell boundaries, where a higher number allows more smoothing. The preferred inversion used  $\gamma = 0.3$  in the horizontal directions and  $\gamma = 0.4$  in the vertical direction, thereby allowing for lateral resistivity variations that were less smooth than variations with depth. The model had a tear halfway through the sedimentary basins of the upper crust, as determined by the CRUST 1.0 model (Laske et al., 2013), meaning that  $\gamma$  was reduced to zero at model cell interfaces corresponding to half of the sedimentary layer thickness, hence no smoothing was imposed across the tear. This tear allowed for sharp resistivity transitions, as might be expected from the layered sedimentary geology of the WCSB. Typical sedimentary strata in this region are Cretaceous siliciclastic rocks overlying Devonian carbonate rocks; since the latter are more resistive, it is reasonable to place a tear within the sedimentary layer. This initial condition had little effect on the resistivity structure beneath the Cordillera, but it was used because it did affect the resistivity structure beneath the WCSB (not presented here). The inversion started with a regularization parameter ( $\lambda$ ) of 1 and this value decreased, one order of magnitude at a time, to a minimum value of  $10^{-8}$  by the end of the inversion. With high values of  $\lambda$ , the inversion will prioritize a smooth model; with low values of  $\lambda$ , the inversion will prioritize low data misfit. This created smooth models at early iterations, then allowed more complex structures to emerge as the inversion progressed.

Upward of twenty 3-D inversions were run to examine the available data and dependence on control parameters. The preferred inversion used a starting model with 10  $\Omega\cdot\text{m}$  above the tear in the sedimentary rocks and 100  $\Omega\cdot\text{m}$  everywhere else. After 297 iterations, the inversion converged to a root-mean-square (r.m.s.) misfit of 2.23 from a starting value of 16. Additional inversions are currently in progress and the model is yet to be finalized; however, it is unlikely to change significantly.

## Study Area 2: Mount Meager

### Geothermal Background

Study area 2 is centred on Mount Meager (Figure 2), which is the volcano active most recently in the Canadian portion of the GVB, with a major eruption ~2400 years ago (Hickson, 1994). The Mount Meager area drew attention as a geothermal target in the 1970s because of two thermal spring systems: Meager Creek springs and Pebble Creek spring (Souther, 1981). Early exploration work included

geothermometry, DC resistivity surveys and diamond drilling (Fairbank et al., 1981). Lewis and Jessop (1981) measured heat flow of 132 mW/m<sup>2</sup> in a drillhole near Mount Meager, which was elevated compared to a mean of 79 mW/m<sup>2</sup> in three other drillholes, each more than 10 km from Mount Meager. Based on these studies, this volcano is one of the most promising geothermal targets near to infrastructure in Canada, and has been the subject of research since the 1970s (Jessop, 1998). However, a number of barriers to development have been identified and need to be addressed.

One challenge to development at Mount Meager has been the distance to the power grid. This has improved in recent years since Innergex Renewable Energy Inc. (Innergex) has been operating two run-of-river hydroelectric plants near Mount Meager since 2017, as part of their Upper Lillooet River hydro project. Electricity generated at these two facilities is transmitted to the BC Hydro transmission system by a 230 kV transmission line. The proximity of this high-voltage line to Meager Creek has increased the economic feasibility of a geothermal power plant in the area; however, Innergex would be under no obligation to enter a corporate relationship with a geothermal developer. Meager Creek Development Corporation is planning to produce

green hydrogen instead of delivering power to the grid, removing this particular hurdle. Green hydrogen is produced from water by electrolysis using renewable electricity.

Another challenge to development comes from landslide hazards. A large rockslide and debris flow occurred at Mount Meager on August 6, 2010, that displaced 48.5 million cubic metres of material (Guthrie et al., 2012; Allstadt, 2013). Meager Creek was temporarily dammed, and the flood risk led to the evacuation of 1500 residents of Pemberton (Guthrie et al., 2012). Therefore, landslide hazard assessment is an important consideration for ongoing geothermal development at Mount Meager.

A remaining challenge comes from uncertainties in the permeability and porosity of the rocks in the reservoir. This question can be addressed with geophysical studies that image the subsurface structure, as described in this paper.

### Data and Methods

Within study area 2, the available broadband MT data were recorded at 73 stations within an area covered by latitudes 50.48 to 50.74°N and longitudes 123.29 to 123.71°W, as shown in Figure 4. These data included seven soundings collected in 1982 by the Pacific Geoscience Centre (Flores-

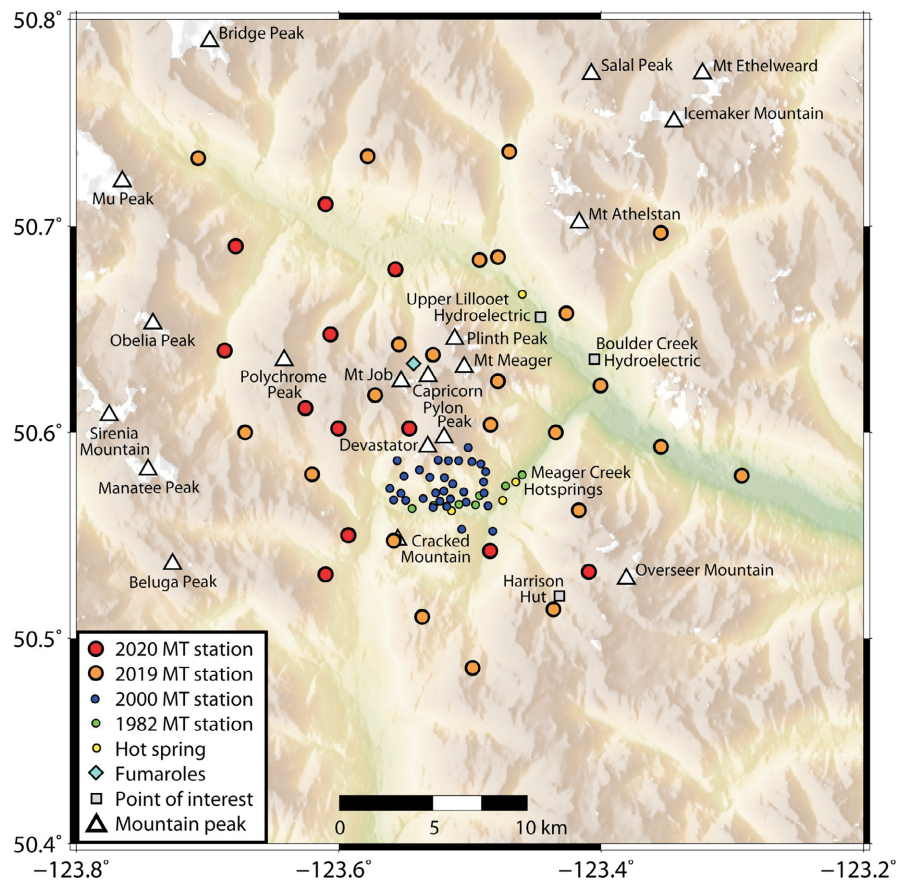


**Figure 4.** Study area 2 showing locations of all 73 available broadband magnetotelluric data sites.

Luna, 1986), 31 soundings collected in 2000 by Frontier Geosciences Inc. (Candy, 2001), and 35 soundings collected by the University of Alberta for this study, 23 sites in 2019 and 12 sites in 2020 (Unsworth et al., 2021). These time series were processed using robust algorithms (Egbert and Eisel, 1998) based on the theory of Egbert and Booker (1986). These frequency-domain data were edited manually to remove outliers.

For this study, a resistivity model was obtained from joint inversion of impedance and tipper data using 29 periods (0.0025–1000 s) and 66 of the 73 available data sites (Figure 5). The data sites consist of two from 1982, 30 from 2000, 22 from 2019 and 12 from 2020. An inversion with 64 data sites (2000–2020 data) and another with 34 data sites (2019–2020 data) will be performed at a later stage in this study to test the robustness of the model and possible influence of time variations; however, 20 to 40 years is a relatively short amount of time when considering the evolution of a magma body and its associated hydrothermal systems (Arnósson, 2014; Karakas et al., 2017).

A 5% relative error floor was applied to the impedance data and a 0.03 absolute error floor was applied to the tipper

data. As for study 1, the ModEM algorithm (Kelbert et al., 2014) was used to invert the data. The inversion started from a 100  $\Omega \cdot m$  half-space with an r.m.s. misfit of 11.7 and converged to a resistivity model with a misfit of 2.0 after 670 iterations.

The 3-D rectangular model mesh used for this study had 2.1 million cells: 148 in the north-south direction, 136 in the east-west direction, and 105 in the vertical direction. The cells were 250 by 250 m in the horizontal plane, with 15 padding cells increasing geometrically by a factor of 1.35 away from the central grid (Figure 5). The upper layers were 50 m thick, then layer thickness increased geometrically by a factor of 1.1 below topography. The top 12 layers, higher than all the MT sites, were removed to decrease the total model size and the computing resources needed.

## Resistivity Models

### Southeastern BC

Although the resistivity model developed for study area 1 extends to depths in excess of 300 km, this paper only presents results for the uppermost 80 km and focuses on crustal features. Attention is drawn to features near the SRMT, and

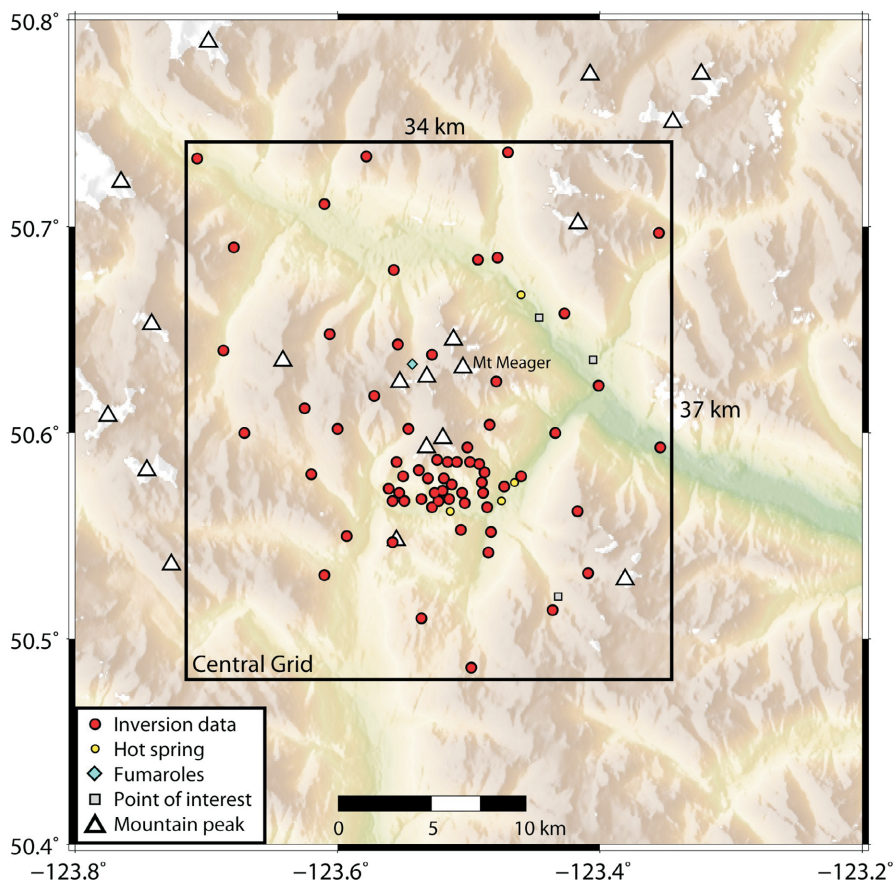


**Figure 5.** Extent of central grid of study area 2 showing locations of the 66 magnetotelluric data sites included in the inversion that produced the resistivity model shown in Figures 8 and 9. Points of interest and mountain peaks are as labelled in Figure 4.

the potential for future geothermal exploration is discussed.

In the model, the Canadian Cordillera in southeastern BC is characterized by resistive upper crust and numerous discrete mid- and lower-crustal conductors. To the east, beneath the plains of Alberta, the high-resistivity North American craton is overlain by the low-resistivity WCSB. Three horizontal slices of the preferred resistivity model are presented in Figure 6.

A band of low resistivity west of the BC–Alberta border is observed at crustal depths of 5–30 km (e.g., Figure 6a–b). This lateral change in resistivity structure corresponds roughly to the well-documented facies boundary between the Paleozoic carbonate platform to the east and the shale-dominated oceanic basin to the west. Rocks in the shale basin are more commonly deformed in a ductile manner, and show pervasive penetrative cleavage and low-grade metamorphism, whereas the eastern carbonate rocks are typically deformed in a brittle manner, and are unmetamorphosed. It has been suggested that the facies boundary is the trace of a continental suture (Johnston, 2008; Chen et al., 2019), which may explain the contrasting electrical properties observed on either side. At depths greater than 25 km, there could be partial melting in the southern Omineca Belt (Ledo and Jones, 2001) and several large conductors extend below this depth in our model (Figure 6c). At shallower depths, low resistivity is more likely caused by interconnected saline fluids. Figure 6c shows the model layer at a depth of 51–58 km, which is close to the depth of the Moho near the SRMT (Bennett et al., 1975).

A cross-section of the resistivity model for study area 1 is presented in Figure 7. The profile A-B-C is roughly parallel to the SRMT (see Figure 3) and passes close to eight thermal springs. The northernmost of them, Canoe River hot spring, is correlated with a large, low-resistivity anomaly that was named the Valemount conductor (VC) in this study. This oblong, northwest-trending crustal conductor is least resistive ( $<1 \Omega \cdot \text{m}$ ) beneath the Canoe River hot spring and is 10–20 km thick for much of its length. To the northwest of the hot spring, the conductor dips at  $\sim 45^\circ$  to a depth of  $\sim 60$  km, and to the southeast it extends horizontally for more than 100 km. The VC is the deepest of the various conductors resolved in our model beneath the SRMT. The depth to the base of a conductor is poorly resolved by the MT method, therefore it cannot be determined if the VC extends into the mantle. It must also be noted that the Moho in Figure 7 is approximated by a straight line at 55 km depth although its depth is likely variable along the profile. The VC is located in the footwall of the SRMT fault, a westward-dipping normal fault. The low resistivity could be caused by saline fluids in porous fractured rocks near the fault and/or conductive minerals (e.g., graphite, sulphides or clays) deposited by prior fluid flow; however, interpretations are still in progress. Lee (2020) interpreted a shallow crustal conductor near the SRMT fault in the same region as more likely caused by graphite or sulphides than aqueous fluids.

The seven hot springs on profile B-C (Figure 7) occur near faults. Wolfenden and Radium hot springs are near the southern end of the Purcell thrust fault and the northern end of the Redwall fault; Fairmont and Red Rock hot springs

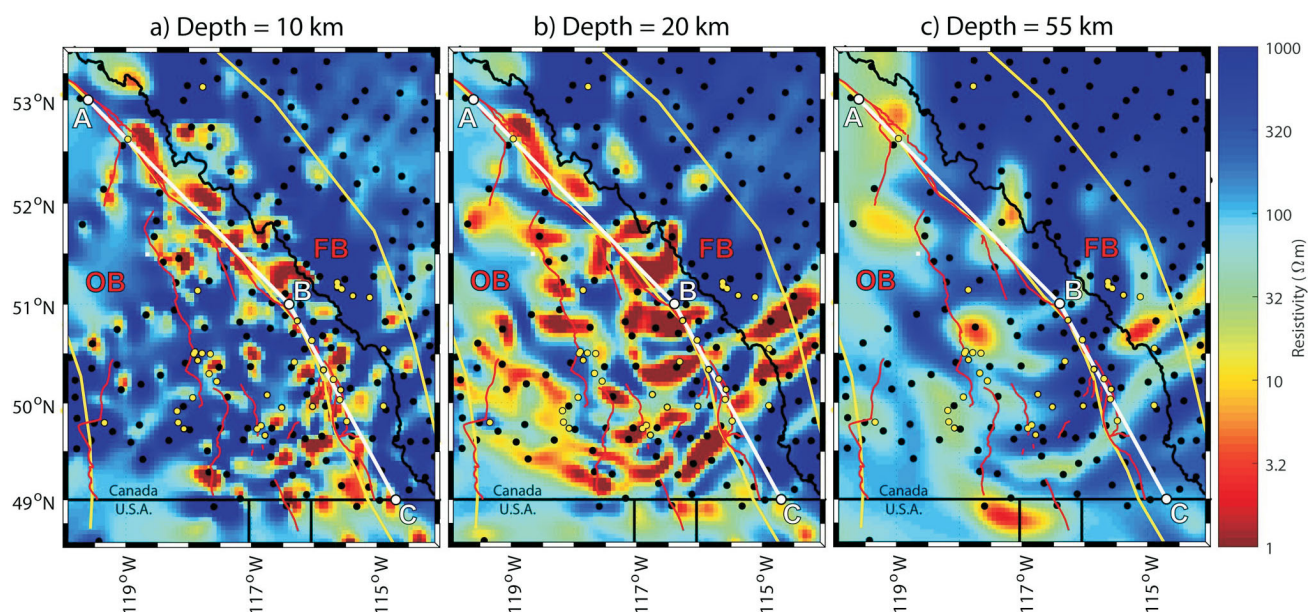


**Figure 6.** Horizontal slices of the resistivity model in the area bounded by latitudes 48.5–53.5°N and longitudes 114–120°W, at depths of **a)** 9–11 km, **b)** 19–22 km, and **c)** 51–58 km. Provincial and federal boundaries (black lines), morphogeological boundaries (yellow lines), surface traces of major faults (red lines), thermal springs (yellow dots) and magnetotelluric sites (black dots) are also shown. Abbreviations: FB, Foreland Belt; OB, Omineca Belt. A cross-section along profile A-B-C is shown in Figure 7.

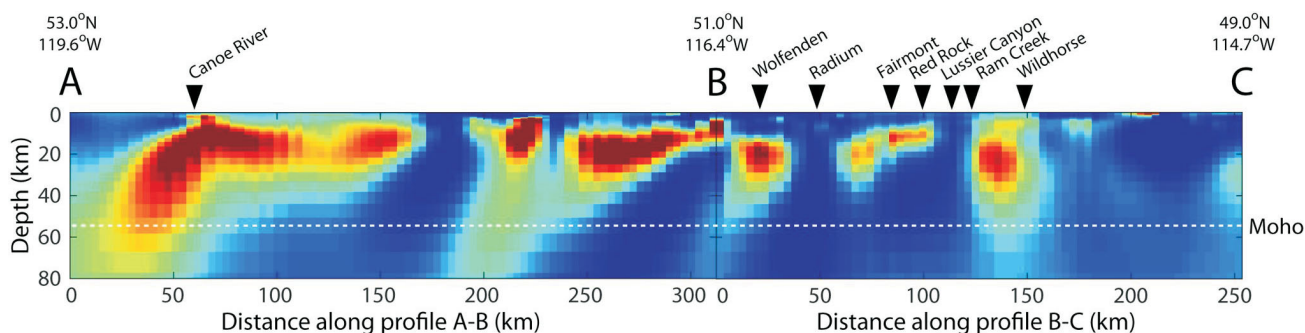


**Figure 7.** Cross-section of the resistivity model for southeastern British Columbia in the vicinity of the southern Rocky Mountain Trench, along with the locations of eight nearby thermal springs. The location of profile A-B-C and the resistivity colour scale are shown in Figure 6. Approximate depth of the Moho (white dashed line at 55 km depth) is from a seismic refraction model (Bennett et al., 1975).

are near the Redwall fault; and Lussier Canyon, Ram Creek and Wildhorse hot springs are near the Lussier River fault. There are a few mid-crustal conductors beneath this cluster of hot springs, predominantly in the 11–33 km depth range (Figure 7). The observed low resistivity is likely caused by aqueous fluids as these depths are within the 400–700°C temperature range (Hyndman and Shearer, 1989; Currie and Hyndman, 2006). The pattern of subparallel, discrete conductors in the middle of profile A-B-C could be caused by electrical anisotropy (e.g., Heise and Pous, 2001) and will be subject to further investigation, such as forward modelling and anisotropic 3-D inversion.

Low resistivity (0.1–10 Ω•m) is observed in the upper and middle crust, extending ~100 km to the northwest from point B, but there is a conspicuous absence of hot springs in this region. This section of the profile is near the Cretaceous Purcell thrust fault, which was not reactivated by Eocene extension nor modern transpression and is therefore likely not permeable. This low-resistivity anomaly is shallowest beneath the Columbia River northwest of Golden, BC. The low resistivity could be caused by conductive minerals deposited by prior fluid flow associated with the extinct Purcell thrust; however, the possibility of saline fluids trapped beneath an impermeable layer or diffused within a permeable layer such that they do not form a discrete hot spring at the surface cannot be excluded. This region is recommended for future geophysical research, for example, a higher-frequency MT survey with shorter inter-station distances. If possible, the resulting dataset should be inverted using a 3-D anisotropic inversion program (e.g., Kong et al., 2021). Conductors associated with other clusters of hot springs, in the central-southern Omineca Belt for example, will be presented and discussed in future publications.

The resistivity model for study area 1 shows broad similarities with previous MT studies in the Canadian Cordillera. Rippe et al. (2013) used 2-D inversion of MT data to create a pair of subparallel resistivity models of the southern Canadian Cordillera, and they imaged a crustal conductor be-

neath the Intermontane and Omineca belts. These authors showed that the mid-crust of the southern Canadian Cordillera was characterized by low resistivity, which was interpreted as most likely a layer of aqueous fluids that may be underlain by partial melt. On their southern profile, the upper surface of the crustal conductor was at a depth of ~20 km; a similar but less pronounced conductor, also at ~20 km depth, was observed on their northern model. These lower crustal conductors were interpreted as saline fluids and/or partial melt, with the weaker northern conductor inferred to be due to the reduced extension. Our model shows a similar crustal conductor, but it is shallower and has a more complex 3-D structure than in the 2-D studies. Rippe et al. (2013) also showed that the low resistivity of the upper mantle was consistent with the presence of a shallow asthenosphere at depths greater than 60 km. This agreed with a lithosphere thickness of 50–60 km concluded by Currie and Hyndman (2006) based on thermal constraints and other observations.

### Mount Meager

The resistivity model for study area 2 is presented in Figures 8 and 9; the model should be considered preliminary, as discussed below in ‘Conclusions’.

The uppermost kilometre of the model has highly variable resistivity. Near Mount Meager, the resistivity is generally low (Figure 8a). This is likely caused by saline aqueous fluids (brines) and hydrothermally altered rock.

There is a large conductor 5 to 8 km below sea level, between Mount Meager and Meager Creek (Figure 8b). It is more than 7 km wide (Figure 9a), more than 10 km long (Figure 9b) and more than 3 km thick. This anomaly is likely caused by brines and partially melted rock, and it occurs beneath the areas investigated with MT in 1982 and 2000 (Figure 4). The finer details of the resistivity model may change as the model is refined, but this large feature is certainly robust.

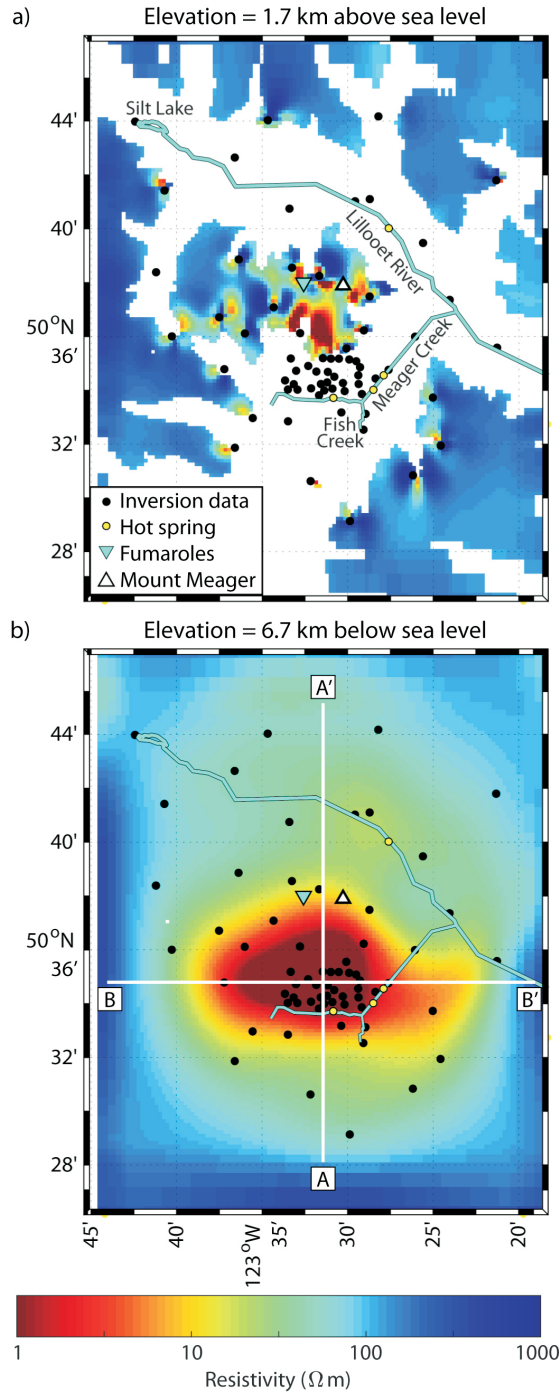


**Figure 8.** Horizontal layers of the 3-D resistivity model for study area 2 at **a)** 1.7 km above sea level, and **b)** 6.7 km below sea level. Cross-sections indicated by lines A-A' and B-B' are shown in Figure 9.

Two general conclusions are very likely at this early stage: 1) there are localized regions of near-surface brines and hydrothermally altered rock beneath the Mount Meager massif, and 2) there is a magma body beneath the Mount Meager massif in the depth range of 7 to 10 km. Detailed

descriptions of these features will require further analysis, but these conclusions are not inconsistent with the last volcanic episode on Mount Meager happening so recently, the degree of hydrothermal alteration seen in the near surface as a result of landslide failures, and the presence of long-

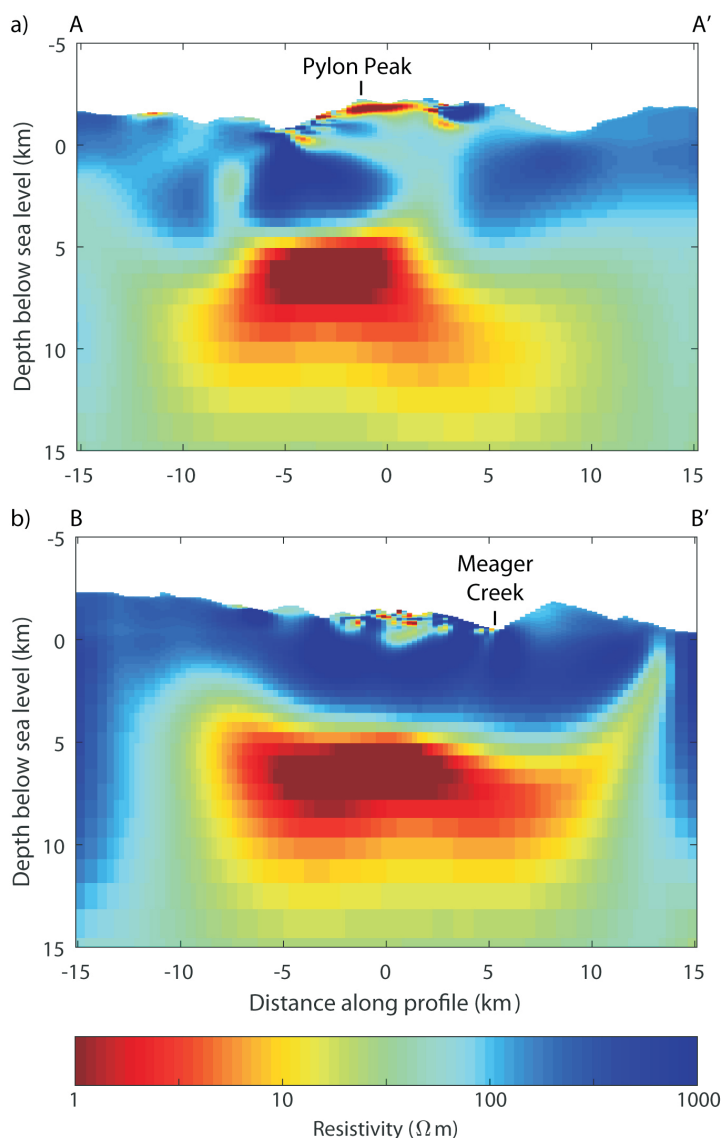


**Figure 9.** Cross-sections of the 3-D resistivity model for study area 2 from **a)** south to north (A-A'), and **b)** west to east (B-B'). Locations of the cross-sections are shown on Figure 8b.

lived fumaroles (Hickson et al., 1999; Stewart et al., 2003; Hickson, 2017). Implications for development of geothermal resources are also being considered.

### Conclusions

The 3-D resistivity model presented in this paper for study area 1 shows that the mid-crustal layer is composed of a number of discrete low-resistivity zones. Some of these appear to underlie regions with known geothermal manifestations, but others do not. It may be that some of these discrete zones are representative of ‘blind’ geothermal systems that do not have surface manifestations. However, the observed pattern may also be indicative of strong crustal anisotropy that is poorly resolved with this isotropic inversion.

As these results are still preliminary, further research is needed in two new directions: 1) application of a new 3-D anisotropic magnetotelluric inversion algorithm to test if the pattern of discrete conductors is caused by electrical anisotropy or a reasonable representation of the geology, and 2) use of denser grids for the magnetotelluric data in areas of interest to detect fluid pathways from the mid-crustal layer to the surface. A finer model mesh and higher frequency data at additional locations would allow the resolution of smaller and shallower features. Two examples of possible target areas are: 1) a region encompassing the Redwall and Lussier River faults, where there are several known hot springs; and 2) the southern Rocky Mountain Trench northwest of Golden, where there is a notable ab-

sence of thermal springs. Modelling of the upper-crustal (e.g., top 5 km) resistivity structure, especially with the addition of topography, could image specific hydrothermal systems associated with known hot springs, and possibly locate potential blind geothermal systems.

The resistivity model presented in this paper for study area 2 is preliminary and the following research steps are currently in progress or being planned: 1) variation of smoothing parameters, e.g., the regularization parameter ( $\lambda$ ) and model covariance length scale ( $\gamma$ ); 2) testing of different data subsets, e.g., without the 1982 and/or 2000 data; and 3) testing of data sensitivity and model resolution, e.g., forward modelling and synthetic inversions.

After the resistivity model has been finalized, more detailed interpretations will be made and will include: 1) estimation of fluid content and relevant parameters using constraints from geophysical and chemical experiments; 2) estimation of melt fraction using constraints from petrological experiments, as was done by Comeau et al. (2015) and Cordell et al. (2018); and 3) joint interpretations using results from the gravity and seismic investigations also being carried out for the Garibaldi volcanic belt geothermal energy project. Audio-magnetotelluric (AMT) data were also collected for this project in 2019 (Craven et al., 2020) and the regional model presented in this paper will assist the AMT interpretations. The two resistivity models, with different spatial scales, will be compared and possibly merged into one.

## Acknowledgments

Funding was provided by a Natural Sciences and Engineering Research Council of Canada Discovery Grant to M.J. Unsworth and an award from the Future Energy Systems program at the University of Alberta. Additional resources and support were provided by Natural Resources Canada and Geoscience BC. The authors are grateful to J.K. Russell for reviewing this paper and thank T. Finley for providing invaluable feedback and discussions; G. Egbert, A. Kelbert and N. Meqbel for use of ModEM; and Compute Canada for access to high-performance cluster computing. The authors also thank S. Grasby, J. Craven, A. Williamson and Z. Vestrum for all of their help; C. Candy at Frontier Geosciences Inc. for access to the 2000 magnetotelluric data; and the outstanding pilots from No Limits Helicopters.

## References

Allen, D.M., Grasby, S.E. and Voormeij, D.A. (2006): Determining the circulation depth of thermal springs in the southern Rocky Mountain Trench, south-eastern British Columbia, Canada using geothermometry and borehole temperature logs; *Hydrogeology Journal*, v. 14, p. 159–172, URL <<https://doi.org/10.1007/s10040-004-0428-z>>.

Allstadt, K. (2013): Extracting source characteristics and dynamics of the August 2010 Mount Meager landslide from broad-

band seismograms: seismic inversion of Mount Meager landslide; *Journal of Geophysical Research: Earth Surface*, v. 118, p. 1472–1490, URL <<https://doi.org/10.1002/jgrf.20110>>.

Arnórsson, S. (2014): The roots of volcanic geothermal systems— Their birth, evolution and extinction; *in Proceedings 5th African Rift Geothermal Conference*, Arusha, Tanzania, 29–31 October 2014, 8 p.

Bennett, G.T., Clowes, R.M. and Ellis, R.M. (1975): A seismic refraction survey along the southern Rocky Mountain Trench, Canada; *Bulletin of the Seismological Society of America*, v. 65, p. 37–54.

Cagniard, L. (1953): Basic theory of the magneto-telluric method of geophysical prospecting; *Geophysics*, v. 18, p. 605–635, URL <<https://doi.org/10.1190/1.1437915>>.

Candy, C. (2001): Crew Development Corporation Report on a magnetotelluric survey, South Meager Geothermal Project, Pemberton, British Columbia (Project FGI-581); report prepared for Frontier Geosciences Inc., 168 p.

Charlesworth, H.A.K. (1959): Some suggestions on the structural development of the Rocky Mountains of Canada; *Journal of the Alberta Society of Petroleum Geologists*, v. 7, p. 249–256.

Chave, A.D. and Jones, A.G. (2012): *The Magnetotelluric Method: Theory and Practice*; Cambridge University Press, Cambridge, U.K., 604 p.

Chen, Y., Gu, Y.J., Currie, C.A., Johnston, S.T., Hung, S.-H., Schaeffer, A.J. and Audet, P. (2019): Seismic evidence for a mantle suture and implications for the origin of the Canadian Cordillera; *Nature Communications*, v. 10, article no. 2249, 10 p., URL <<https://doi.org/10.1038/s41467-019-09804-8>>.

Comeau, M.J., Unsworth, M.J., Ticona, F. and Sunagua, M. (2015): Magnetotelluric images of magma distribution beneath Volcán Uturuncu, Bolivia: implications for magma dynamics; *Geology*, v. 43, p. 243–246, URL <<https://doi.org/10.1130/G36258.1>>.

Cordell, D., Unsworth, M.J. and Díaz, D. (2018): Imaging the Laguna del Maule Volcanic Field, central Chile using magnetotellurics: evidence for crustal melt regions laterally-offset from surface vents and lava flows; *Earth and Planetary Science Letters*, v. 488, p. 168–180, URL <<https://doi.org/10.1016/j.epsl.2018.01.007>>.

Craven, J.A., Hormozzade, F., Tschirhart, V., Ansari, M., Bryant, R. and Montezadian, D. (2020): Overview of the 2019 audiomagnetotelluric survey of the Mount Meager geothermal reservoir; Chapter 6 *in Garibaldi Geothermal Energy Project, Mount Meager 2019 - Field Report*, Geoscience BC, Report 2020-09, p. 126–147, URL <<https://https://geoscan.nrcan.gc.ca/starweb/geoscan/servlet.starweb?path=geoscan/fulle.web&search1=R=326818>> [October 2021].

Currie, C.A. and Hyndman, R.D. (2006): The thermal structure of subduction zone back arcs; *Journal of Geophysical Research: Solid Earth*, v. 111, URL <<https://doi.org/10.1029/2005JB004024>>.

Egbert, G.D. and Booker, J.R. (1986): Robust estimation of geoelectrical transfer functions; *Geophysical Journal International*, v. 87, p. 173–194, URL <<https://doi.org/10.1111/j.1365-246X.1986.tb04552.x>>.

Egbert, G.D. and Eisel, M. (1998): EMTF: Programs for robust single station and remote reference analysis of magnetotelluric data: UNIX (and PC) version; software manual, 35 p.

- Fairbank, B.D., Openshaw, R.E., Souther, J.G. and Stauder, J.J. (1981): Meager Creek Geothermal Project: an exploration case history; *Geothermal Resources Council Bulletin*, v. 10, p. 3–7, URL <<https://doi.org/10.4095/103409>>.
- Finley, T. (2020): Fault-hosted geothermal systems in southeastern British Columbia; M.Sc. thesis, University of Alberta, 208 p.
- Flores-Luna, C.F. (1986): Electromagnetic induction studies over the Meager Creek geothermal area, British Columbia; Ph.D. thesis, University of Toronto, 222 p.
- Foo, W.K. (1979): Evolution of transverse structures linking the Purcell Anticlinorium to the western Rocky Mountains near Canal Flats, British Columbia; Ph.D. thesis, Queen's University, 146 p.
- Frost, B.R., Fyfe, W.S., Tazaki, K. and Chan, T. (1989): Grain-boundary graphite in rocks and implications for high electrical conductivity in the lower crust; *Nature*, v. 340, p. 134–136, URL <<https://doi.org/10.1038/340134a0>>.
- Gal, L.P. and Ghent, E.D. (1990): Metamorphism in the Solitude Range, southwestern Rocky Mountains, British Columbia: comparison with adjacent Omineca Belt rocks and tectonometamorphic implications for the Purcell Thrust; *Canadian Journal of Earth Sciences*, v. 27, p. 1511–1520, URL <<https://doi.org/10.1139/e90-161>>.
- Grasby, S.E. and Ferguson, G. (2010): Controls on the distribution of thermal springs in the Canadian Cordillera; *in Proceedings World Geothermal Congress 2010, Bali, Indonesia, 25–29 April 2010*, 4 p.
- Grasby, S.E. and Hutcheon, I. (2001): Controls on the distribution of thermal springs in the southern Canadian Cordillera; *Canadian Journal of Earth Sciences*, v. 38, p. 427–440.
- Grasby, S.E., Ansari, S.M., Calahorrano-Di Patre, A., Chen, Z., Craven, J.A., Dettmer, J., Gilbert, H., Hanneson, C., Harris, M., Liu, J., Muhammad, M., Russell, K., Salvage, R.O., Savard, G., Tschirhart, V., Unsworth, M.J., Vigouroux-Caillibot, N. and Williams-Jones, G. (2020): Geothermal resource potential of the Garibaldi volcanic belt, southwestern British Columbia (part of NTS 092J); *in Geoscience BC Summary of Activities 2019: Energy and Water*, Geoscience BC, Report 2020-02, p. 103–108, URL <[https://www.geosciencebc.com/i/pdf/SummaryofActivities2019/EW/Project%202018-004\\_EW\\_SOA2019.pdf](https://www.geosciencebc.com/i/pdf/SummaryofActivities2019/EW/Project%202018-004_EW_SOA2019.pdf)> [October 2021].
- Guthrie, R.H., Friele, P., Allstadt, K., Roberts, N., Evans, S.G., Delaney, K.B., Roche, D., Clague, J.J. and Jakob, M. (2012): The 6 August 2010 Mount Meager rock slide-debris flow, Coast Mountains, British Columbia: characteristics, dynamics, and implications for hazard and risk assessment; *Natural Hazards and Earth System Sciences*, v. 12, p. 1277–1294, URL <<https://doi.org/10.5194/nhess-12-1277-2012>>.
- Heise, W. and Pous, J. (2001): Effects of anisotropy on the two-dimensional inversion procedure; *Geophysical Journal International*, v. 147, p. 610–621, URL <<https://doi.org/10.1046/j.0956-540x.2001.01560.x>>.
- Hersir, G.P., Árnason, K. and Vilhjálmsson, A.M. (2015): 3D inversion of magnetotelluric (MT) resistivity data from Krýsuvík high temperature geothermal area in SW Iceland; *in Proceedings World Geothermal Congress 2015, Melbourne, Australia, 19–25 April 2015*, 14 p.
- Hickson, C.J. (1994): Character of volcanism, volcanic hazards, and risk, northern end of the Cascade magmatic arc, British Columbia and Washington State; *Geological Survey of Canada, Bulletin 481*, p. 231–250, URL <<https://doi.org/10.4095/203253>>.
- Hickson, C.J. (2017): Mount Meager data compilation; Geoscience BC, Project 2017-006, URL <<http://www.geosciencebc.com/projects/2017-006/>> [October 2021].
- Hickson, C.J., Russell, J.K. and Stasiuk, M.V. (1999): Volcanology of the 2350 B.P. eruption of Mount Meager Volcanic Complex, British Columbia, Canada: implications for hazards from eruptions in topographically complex terrain; *Bulletin of Volcanology*, v. 60, p. 489–507, URL <<https://doi.org/10.1007/s004450050247>>.
- Hutchinson, J., Kao, H., Riedel, M., Obana, K., Wang, K., Kodaira, S., Takahashi, T. and Yamamoto, Y. (2020): Significant geometric variation of the subducted plate beneath the northernmost Cascadia subduction zone and its tectonic implications as revealed by the 2014 MW 6.4 earthquake sequence; *Earth and Planetary Science Letters*, v. 551, article no. 116569, 11 p., URL <<https://doi.org/10.1016/j.epsl.2020.116569>>.
- Hyndman, R.D. and Shearer, P.M. (1989): Water in the lower continental crust: modelling magnetotelluric and seismic reflection results; *Geophysical Journal International*, v. 98, p. 343–365, URL <<https://doi.org/10.1111/j.1365-246X.1989.tb03357.x>>.
- Jessop, A.M. (1998): Geothermal energy in Canada; *Geoscience Canada*, v. 25, p. 33–41.
- Johnston, S.T. (2008): The Cordilleran ribbon continent of North America; *Annual Review of Earth and Planetary Sciences*, v. 36, p. 495–530, URL <<https://doi.org/10.1146/annurev.earth.36.031207.124331>>.
- Karakas, O., Degruyter, W., Bachmann, O. and Dufek, J. (2017): Lifetime and size of shallow magma bodies controlled by crustal-scale magmatism; *Nature Geoscience*, v. 10, p. 446–450, URL <<https://doi.org/10.1038/ngeo2959>>.
- Kelbert, A., Meqbel, N., Egbert, G.D. and Tandon, K. (2014): ModEM: a modular system for inversion of electromagnetic geophysical data; *Computers & Geosciences*, v. 66, p. 40–53, URL <<https://doi.org/10.1016/j.cageo.2014.01.010>>.
- Kong, W., Tan, H., Lin, C., Unsworth, M., Lee, B., Peng, M., Wang, M. and Tong, T. (2021): Three-dimensional inversion of magnetotelluric data for a resistivity model with arbitrary anisotropy; *Journal of Geophysical Research: Solid Earth*, v. 126, issue 8, August 2021, e2020JB020562, URL <<https://doi.org/10.1029/2020JB020562>>.
- Kreemer, C., Blewitt, G. and Klein, E.C. (2014): A geodetic plate motion and global strain rate model; *Geochemistry, Geophysics, Geosystems*, v. 15, p. 3849–3889, URL <<https://doi.org/10.1002/2014GC005407>>.
- Laske, G., Masters, G., Ma, Z. and Pasyanos, M. (2013): Update on CRUST1.0 - A 1-degree global model of Earth's crust; *Geophysical Research Abstracts*, v. 15, Abstract EGU2013-2658, URL <<http://igppweb.ucsd.edu/~gabi/rem.html>> [November 2021].
- Ledo, J. and Jones, A.G. (2001): Regional electrical resistivity structure of the southern Canadian Cordillera and its physical interpretation; *Journal of Geophysical Research: Solid Earth*, v. 106, p. 30755–30769, URL <<https://doi.org/10.1029/2001JB000358>>.
- Lee, B. (2020): Improving exploration for geothermal resources with the magnetotelluric method; Ph.D. thesis, University of Alberta, 288 p.
- Lewis, J.F. and Jessop, A.M. (1981): Heat flow in the Garibaldi volcanic belt, a possible Canadian geothermal energy resource area; *Canadian Journal of Earth Sciences*, v. 18, p. 366–375, URL <<https://doi.org/10.1139/e81-028>>.
- Lindsey, N.J. and Newman, G.A. (2015): Improved workflow for 3D inverse modeling of magnetotelluric data: examples from

- five geothermal systems; *Geothermics*, v. 53, p. 527–532, URL <<https://doi.org/10.1016/j.geothermics.2014.09.004>>.
- Majorowicz, J. and Grasby, S.E. (2010): Heat flow, depth–temperature variations and stored thermal energy for enhanced geothermal systems in Canada; *Journal of Geophysics and Engineering*, v. 7, p. 232–241, URL <<https://doi.org/10.1088/1742-2132/7/3/002>>.
- McDonough, M.R. and Simony, P.S. (1988): Structural evolution of basement gneisses and Hadrynian cover, Bulldog Creek area, Rocky Mountains, British Columbia; *Canadian Journal of Earth Sciences*, v. 25, p. 1687–1702, URL <<https://doi.org/10.1139/e88-159>>.
- McMechan, M.E. and Thompson, R.I. (1989): Structural style and history of the Rocky Mountain fold and thrust belt; Chapter 4 in *Western Canada Sedimentary Basin: A Case History*, Canadian Society of Petroleum Geologists, p. 47–71.
- Meqbel, N.M., Egbert, G.D., Wannamaker, P.E., Kelbert, A. and Schultz, A. (2014): Deep electrical resistivity structure of the northwestern U.S. derived from 3-D inversion of USArray magnetotelluric data; *Earth and Planetary Science Letters*, v. 402, p. 290–304, URL <<https://doi.org/10.1016/j.epsl.2013.12.026>>.
- Mullen, E.K., Weis, D., Marsh, N.B. and Martindale, M. (2017): Primitive arc magma diversity: new geochemical insights in the Cascade Arc; *Chemical Geology*, v. 448, p. 43–70, URL <<https://doi.org/10.1016/j.chemgeo.2016.11.006>>.
- Muñoz, G. (2014): Exploring for geothermal resources with electromagnetic methods; *Surveys in Geophysics*, v. 35, p. 101–122, URL <<https://doi.org/10.1007/s10712-013-9236-0>>.
- North, F.K. and Henderson, G.G.L. (1954): The Rocky Mountain Trench; in *Guide Book, Fourth Annual Field Conference, Banff–Golden–Radium*, Canadian Society of Petroleum Geologists, p. 82–100.
- Rippe, D., Unsworth, M.J. and Currie, C.A. (2013): Magnetotelluric constraints on the fluid content in the upper mantle beneath the southern Canadian Cordillera: implications for rheology; *Journal of Geophysical Research: Solid Earth*, v. 118, p. 5601–5624, URL <<https://doi.org/10.1002/jgrb.50255>>.
- Souther, J.G. (1981): Canadian Geothermal Research Program; in *Energy Resources of the Pacific Region*, AAPG Studies in Geology, v. 12, p. 391–400.
- Stern, R.J. (2002): Subduction zones; *Reviews of Geophysics*, v. 40, p. 3-1–3-38, URL <<https://doi.org/10.1029/2001RG000108>>.
- Stewart, M.L., Russell, J.K. and Hickson, C.J. (2003): Discrimination of hot versus cold avalanche deposits: implications for hazard assessment at Mount Meager, B.C.; *Natural Hazards and Earth System Sciences*, v. 3, p. 713–724, URL <<https://doi.org/10.5194/nhess-3-713-2003>>.
- Tuya Terra Geo Corp. and Geothermal Management Company, Inc. (2016): Direct-use geothermal resources in British Columbia, Section A: Summary of findings; Geoscience BC, Report 2016-07, 38 p., URL <<http://www.geosciencebc.com/projects/2015-022/>> [October 2021].
- Unsworth, M.J., Hanneson, C., Williamson, A.R. and Vestrum, Z.E. (2021): Final report on the 2019-2020 broadband magnetotelluric study at Mount Meager: implications for structure of the hydrothermal and magmatic system; Chapter 5 in *Garibaldi Geothermal Energy Project - Phase 1: Final Report*, Geoscience BC, Report 2021-08, p. 79–146, URL <[http://www.geosciencebc.com/i/project\\_data/GBCReport2021-08/GBCR%202021-08%20Garibaldi%20Geothermal%20Energy%20Project%20%20Phase%201.pdf](http://www.geosciencebc.com/i/project_data/GBCReport2021-08/GBCR%202021-08%20Garibaldi%20Geothermal%20Energy%20Project%20%20Phase%201.pdf)> [October 2021].
- Ussher, G., Harvey, C., Johnstone, R. and Anderson, E. (2000): Understanding the resistivities observed in geothermal systems; in *Proceedings World Geothermal Congress 2000, Kyushu - Tohoku, Japan, May 28–June 10, 2000*, p. 1915–1920.
- van der Velden, A.J. and Cook, F.A. (1996): Structure and tectonic development of the southern Rocky Mountain trench; *Tectonics*, v. 15, p. 517–544, URL <<https://doi.org/10.1029/95TC03288>>.
- Varentsov, I.M., Kulikov, V.A., Yakovlev, A.G. and Yakovlev, D.V. (2013): Possibilities of magnetotelluric methods in geophysical exploration for ore minerals; *Izvestiya, Physics of the Solid Earth*, v. 49, p. 309–328, URL <<https://doi.org/10.1134/S1069351313030178>>.
- Wang, E. (2019): Multidimensional magnetotelluric studies of the Precambrian Alberta basement; Ph.D. thesis, University of Alberta, 397 p.
- Wisian, K.W. and Blackwell, D.D. (2004): Numerical modeling of Basin and Range geothermal systems; *Geothermics*, v. 33, p. 713–741.

